



Influence of the layer thickness in plasmonic gold nanoparticles produced by thermal evaporation

D. Gaspar¹, A. C. Pimentel¹, T. Mateus¹, J. P. Leitão², J. Soares², B. P. Falcão², A. Araújo¹, A. Vicente¹, S. A. Filonovich¹, H. Águas¹, R. Martins¹ & I. Ferreira¹

¹CENIMAT/I3N, Departamento de Ciência dos Materiais and CEMOP/UNINOVA, Faculdade de Ciências e Tecnologia, Universidade Nova de Lisboa, 2829-516 Caparica, Portugal, ²Departamento de Física and I3N, Universidade de Aveiro, 3810-193 Aveiro, Portugal.

Metallic nanoparticles (NPs) have received recently considerable interest of photonic and photovoltaic communities. In this work, we report the optoelectronic properties of gold NPs (Au-NPs) obtained by depositing very thin gold layers on glass substrates through thermal evaporation electron-beam assisted process. The effect of mass thickness of the layer was evaluated. The polycrystalline Au-NPs, with grain sizes of 14 and 19 nm tend to be elongated in one direction as the mass thickness increase. A 2 nm layer deposited at 250 °C led to the formation of Au-NPs with 10-20 nm average size, obtained by SEM images, while for a 5 nm layer the wide size elongates from 25 to 150 nm with a mean at 75 nm. In the near infrared region was observed an absorption enhancement of amorphous silicon films deposited onto the Au-NPs layers with a corresponding increase in the PL peak for the same wavelength region.

Plasmonic nanoparticles emerged recently as a possible solution to enhance solar cells efficiency¹⁻⁴. High losses of photons due to both incomplete absorption of solar spectrum and thermalization are the main drawbacks that have been addressed to overcome limitations in photovoltaics efficiency. Over the past decades several improvements in solar cells were introduced but the highest conversion efficiency achieved so far for a single junction cell is 25% for crystalline silicon and 10.5% for amorphous silicon⁵.

Surface Plasmon Resonance (SPR) arises in metal NPs as a collective oscillation of the surface electrons when subjected to the electric field associated to the incident light. Also, NPs should be smaller than the wavelength of the incident light in order to achieve SPR. As a result, the nanoparticles polarize. The scattering and absorption of light depends on the polarizability of the NPs, which is a function of the size, refractive index, shape, density and surrounding medium, as demonstrated in several theoretical studies^{6,7}. These parameters should be tuned in order to maximize the NPs light scattering, relatively to absorption. Scattering efficiencies lower than 50% may lead to heat dissipation and absorption suppression. This promotes undesired reduction of photocurrent for solar cells having high response in the blue region⁸. However a change in shape from spherical to ellipsoidal or a change in the NPs medium affects the polarizability with possible red shift in the resonance frequency. In this case, NPs used as front electrode lead to an enhancement of the intrinsic layer absorption above 59% in the infrared region⁹.

The influence of shape: spheroid¹⁰, cylindrical¹¹, nanowires¹², size⁶ and also the distribution¹³ have been studied mainly for Au and Ag nanoparticles. Other nanoparticles such as Sn^{14,15} and ZnO(Al)¹⁶ were also investigated. The chemical synthesis¹⁷, physical vapour deposition with post-deposition annealing¹⁸ or template and electrodeposition^{13,14} are the main production processes. The control of NPs distribution has been obtained by mask template^{13,14}, light manipulation¹⁹ and implantation with focused ion beam lithography²⁰. Those techniques require sophisticated and complex processes limiting direct incorporation of NPs into the required layers of solar cells. We report a simple and compatible process (thermal evaporation assisted by electron-beam) to deposit inter and intra-layers of NPs directly into the amorphous silicon solar cell.

Results

Influence of the layer thickness. SEM images of the Au layers with 2, 5 and 7 nm mass thicknesses, reproducible with ± 0.5 nm variation, are shown in Figure 1a. Clearly, the mass thickness has remarkable impact on the

SUBJECT AREAS:

NANOPARTICLES

SYNTHESIS AND PROCESSING

NANOPHOTONICS AND
PLASMONICS

STRUCTURAL PROPERTIES

Received
10 December 2012

Accepted
6 February 2013

Published
3 April 2013

Correspondence and
requests for materials
should be addressed to
I.F. (imf@fct.unl.pt)

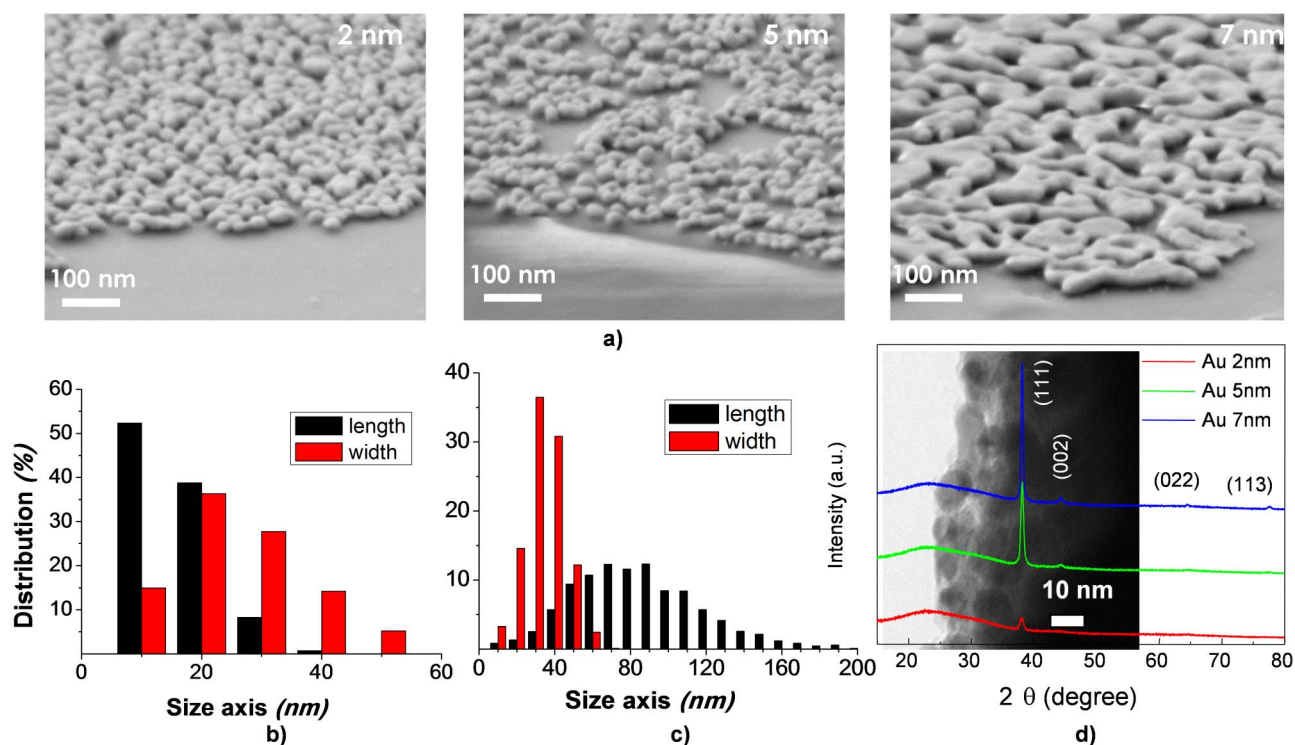


Figure 1 | (a) Tilt (30°) SEM images of Au-NPs deposited on glass substrates for different nominal layer thicknesses (2, 5 and 7 nm) at a substrate temperature of 250°C. (b) Size distribution for the 2 nm Au-NPs layer; (c) Size distribution for the 5 nm Au-NPs layer; (d) XRD patterns of the Au-NPs for different layer thickness and the inset is the TEM image of Au NPs for the 2 nm layer.

coalescence of NPs. The 2 nm layer shows uniform NPs distribution with mean sizes (obtained with the free Image J software) in the range of 10–30 nm (Fig. 1b) while for 5 nm layer the NPs tend to coalesce and form clusters. The size of the clusters is in the range of 10–200 nm with mean of 60–90 nm (Fig. 1c). For the 7 nm mass thickness we observe an enlargement of the clusters that are now linked to each other forming a film with a large open area fraction. The XRD spectra of Au-NPs show a typical pattern of Au cubic structure with a (111) main diffraction peak (Fig. 1d). As expected the peak intensity increases as the layer thickness increases and the grain size determined by the Scherrer formula is 14, 19 and 28 nm, respectively for the 2, 5 and 7 nm mass thicknesses. The inset of figure 1d shows the TEM image of 2 nm Au-NPs produced directly on the Cu TEM grid (400 nm mesh). There, we observe circular grain sizes (<20 nm) that are in agreement with the SEM results and also with the crystallite size obtained from XRD pattern (Fig. 1d). For the Au-NPs with higher thicknesses, the average dimensions obtained from SEM results (Fig. 1c) are clearly higher than the grain sizes estimated by the Scherrer formula which suggests that the Au-NPs for these two films are polycrystalline.

The specular transmittance (T_{sp}), total transmittance (T_T) and reflectance (R) of the different Au -NPs layers are shown in Figure 2a. We observe a decrease in transmittance as the Au mass thickness increases, as expected for a metallic layer. T_T and T_{sp} spectra coincide for both 2 and 5 nm layers while the diffused light is enhanced for higher mass thickness (7 nm). The typical resonance peak of Au-NPs is present but the absorbance is superior for the 5 nm mass thickness layer, disappearing for thicker layers. The reflectance of these layers is inferior to 20% with a slight peak located at the same wavelength of the resonance peak.

a-Si:H with Au-NPs. The transmittance spectra of a-Si:H films with and without Au-NPs are shown in Figure 3a. The absorbance shows a clear improvement in the near infrared region (600–1000 nm) for a-Si:H films deposited on 5 nm Au-NPs layers. The different spectra

displayed in the figure are related to specular and total transmittance obtained with light incidence in the substrate or in the a-Si:H film. The spectra are in good match so no influence of glass/Au-NPs interface is seen. The spectra of a-Si:H with 7 nm layer Au-NPs is not displayed since the absorption of the metallic layer is too high (as shown in Fig. 2a) to be used efficiently in intra layer of solar cells. On the other hand, the a-Si:H films deposited on 2 nm Au-NPs layer show lower absorption and for clarity was also not displayed. The top view SEM images shown in Figure 3b and 3c exhibit the surface morphology of a-Si:H films deposited on glass (Fig. 3b) and on glass with 2 nm layer of Au-NPs (Fig. 3c). The only change observed is a small enlargement of the granular texture of the a-Si:H when deposited on the Au-NPs (2 nm layer).

The optical properties of the Au-NPs and Au-NPs/a-Si:H samples, were investigated through photoluminescence measured at 70 K in the visible and infrared regions as shown in Figure 4. In the first

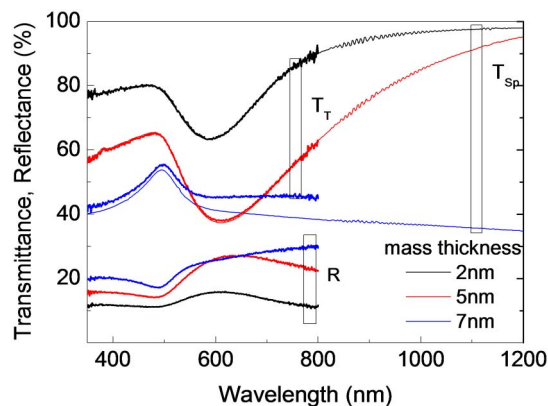


Figure 2 | Transmittance (total- T_T and specular- T_{sp}) and reflectance (R) of Au-NPs layers with different thicknesses.

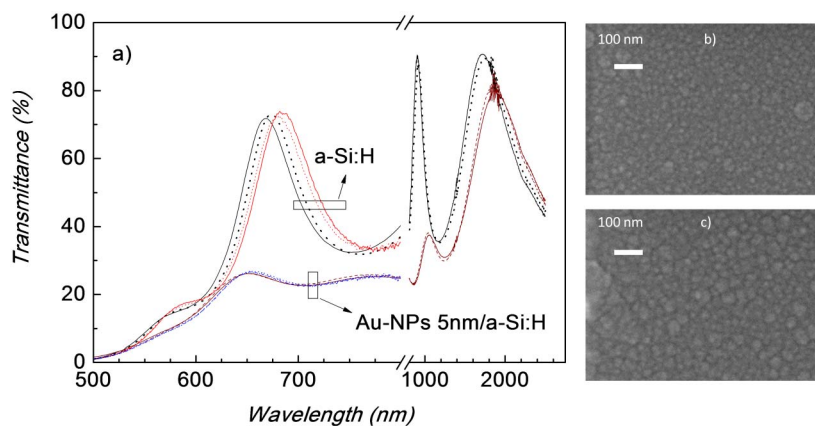


Figure 3 | (a) Transmittance of a-Si:H films without and with Au-NPs. The different lines represent the T_T (red/purple line) and T_{Sp} spectra (black/brown line) obtained by illuminating the samples through the glass (full line) or through the film (dot line); top view SEM images of (b) 200 nm a-Si:H film, and (c) Au-NPs (5 nm)/a-Si:H layers.

region, the measured spectra show a low signal to noise ratio (Figure 4a). For the sample with the nominal 2 nm Au-NPs deposition, a peak centred at ~ 490 nm is observed. By increasing the thickness of the Au-NPs layer, the above peak shifts to higher wavelengths as shown by the arrows in Figure 4a. The SEM images (Fig. 1a) show that the average dimensions of the Au-NPs increase with the raise of the thickness of the deposited Au layer. These peaks corresponds to the interband radiative transitions involving electrons in the sp-conduction band and holes in the d-band^{21–23}.

On the other hand, in the infrared region the spectra evidence a higher signal to noise ratio. The emission is dominated by an asymmetric large band with maximum at ~ 924 nm. The shape of that band for the lower wavelengths could be determined by the low detectivity of the Ge detector in that region. This band can be described by intraband radiative transitions in the sp-conduction band. We observe a decrease of the relative intensity of the emission with the increase of the average size of the Au-NPs. For comparison in Figure 4b we show also the spectra measured for samples in which the a-Si:H layers were deposited directly on top of a glass substrate covered with the nanoparticles shown in Figure 1. The relative intensities between Au-NPs samples with and without a-Si:H layer decrease for 2 nm layer Au-NPs, but increase for those deposited on 5 nm and 7 nm layer.

Discussion

Our study shows the effect of layer thickness on the formation and characteristics of Au-NPs deposited by thermal evaporation. Here, we kept the substrate temperature at 250°C to favour the coalescence of nanoparticles during the deposition of the Au layer and to avoid the usual post deposition thermal annealing step²⁴. As reported recently by Sun et al.²⁴, the morphology of a 5 nm layer, deposited by thermal evaporation, without substrate heating, is porous like interconnected islands and after rapid annealing up to 700°C it tends to form spheroid-like NPs. Thus we have obtained similar shape in 2 nm layers but at a much lower temperature. The Au-NPs formed in the 2 nm deposited layers have mean size of 20–30 nm along one axis, and 30–40 nm along the second direction. The 5 nm thick Au layer deposited at 250°C resulted in NPs clusters with mean size around 30–40 nm in one direction and the second direction elongates towards 60–90 nm. For the 7 nm layer, the NPs are linked, leading to porous films. Also it is worth noting the polycrystalline character of Au-NPs, the XRD data shows the typical cubic structure of Au with grain sizes of 14, 19 and 28 nm, respectively, for 2, 5 and 7 nm mass thickness, which agrees with the average size of an axis (10–15 nm) as determined from SEM and TEM images for the 2 nm layer. According to the results obtained, the Au-NPs are formed with a low number of monolayers by islands growth (Vollmer-Weber,

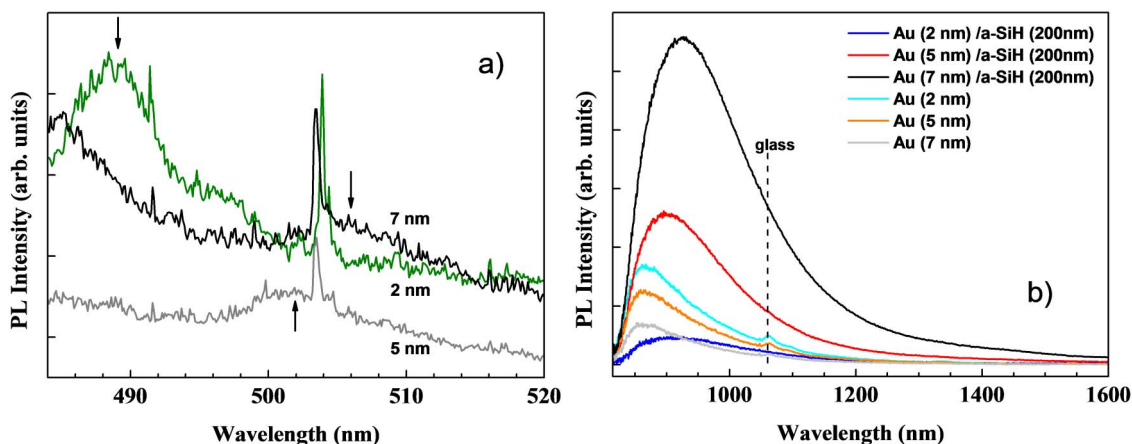


Figure 4 | PL spectra performed at 70 K in a-Si:H thin films with an Au-NPs layer in the visible (a) and infrared (b) regions. The excitation source was the 457 nm laser line in (a) and the 514.5 nm laser line in (b). In (a) the arrows indicate in each spectrum the interband radiative transitions involving electrons in the sp-conduction band and holes in the d-band. The sharp peaks in the region 503–504 nm correspond to radiative transitions from spurious illumination in the room.



VW) process²⁵. This process prevails when the contact angle between the deposited material and the substrate is superior to zero, which means that elastic strain of the film exceeds the adhesion force. However, this process occurs until the number of monolayers is sufficient to change the free enthalpy and the supersaturation parameter, which is one of the driving forces to form a film²⁵. But the formation of Au-NPs depends of the nucleation sites available at the substrate, and these are enhanced when temperature rises. Thus, the thermal evaporation with heated substrate is a suitable process for inclusion of NPs in inter or intra-layers during the deposition of amorphous silicon solar cells.

The transmittance spectra of 2 nm layer revealed an absorption peak at 607 nm consistent with plasmonic resonance of spheroidal NPs (20–30 nm) having low dispersion in their size. For the 5 nm layer the absorption peak shows a red shift from 607 nm to 628 nm and a broadening (FWHM from 129 to 203 nm), which is related to enlargement of the NPs as shown in figure 1. Several authors reported the effect of size, shape, density and surrounding medium of NPs on the plasmonic peak¹³. For instance, Halas et al.²⁶ reported a sharp plasmonic peak at 550 nm for Au spherical NPs, 20 nm of radius, with a sparse distribution, while in a more dense distribution the resonance peak shows a red shift to 750 nm attributed to an interparticle coupling, which is consistent with the Au-NPs clusters observed in the SEM image. If two NPs are close enough they can form a plasmonic dimer with a red shift that depends on the interaction distance between the two particles. This behaviour reflects the near field interactions between two close metallic nanoparticles: near-field coupling and far-field dipolar interactions. Their s- and p- polarization is dependent on the separation and size⁶. Besides particles density, the shape also plays a crucial role in the plasmonic resonance. Alok et al.²⁷, showed that enlarged NPs have two resonant peaks and their relative intensity depends if the particles are elongated perpendicular or parallel to the substrate. These results are in concordance with those found in metallic nanorods where the plasmonic resonance splits into low- and high-energy absorption bands where the high-energy bands correspond to electron transitions perpendicular to the major axis (transverse surface plasmon) and the low-energy bands are related to the transitions along the major axis (longitudinal surface plasmon). The peaks position is also affected by the ratio between the two axes of the nanorods¹². Similar results were also presented by Nakayama et al.¹³. Our results, do not show a clear separation of the different modes so the enhancement and red shift of resonance peak may have equal contribution of both transversal and longitudinal enlargement of NPs. Comparing to the literature we expect a resonance peak of Au-NPs close to 550 nm, as stated before. Several contributions can lead to a red shift of this peak, among those mentioned above we also have to include the effect of the glass substrate. Indeed, Kelly et al.⁶ have reported a red shift of the resonance peak, from 360 nm to 400 nm, as the Ag-NPs are isolated or are covering partially a mica substrate.

Overall, our transmittance results reflect the contributions of an inhomogeneous distribution and surface coverage and the influence of glass substrate.

The deposition of a-Si:H films on the top of nanoparticles leads to an increase in the absorption close to near-infrared wavelength which is adequate for solar cells applications. Although the results of reflectance were not shown by clarity of the graph, it is not influenced by the Au-NPs (in wavelength range of 400–800 nm). Thus, our results show an enhancement in the absorption of a-Si:H when the film is deposited on 5 nm Au-NPs layer. Similar results were reported for Ag-NPs, deposited by thermal evaporation followed by annealing, on polished silicon with a 30 nm oxide layer, being a strong absorption observed for wavelengths above 1000 nm. There, it is shown the increase of absorption with increasing particle diameter¹. Akimov et al.⁹ has also shown an enhancement of light absorption up to 59% when Al-NPs were deposited on the top of

the TCO layer of a-Si:H solar cells. Nevertheless, our Au-NPs are embedded in a-Si:H film and the prove is the coincidence of T_T and T_{Sp} spectra obtained by irradiating the samples from the glass side or from a-Si:H film side (reflectance was not shown also because no difference was observed). As reported by Pillai and Green², if a semiconductor is close to electric field of an emitting dipole, the absorption is enhanced. Other non-linear processes such as up/down-conversion can be originated by the enhancement of electric field around the surface plasmons. In our results the photoluminescence shows that down-conversion (in terms of energy) is obtained in a-Si:H films deposited on Au-NPs (5 nm Au layer). In the literature, the luminescence of Au-NPs, deposited on glass substrate, has shown a red shift of the peak in the visible wavelength range, which was attributed to the reduction in quantum confinement of Au nanoparticles²⁸. Due to the excitation energy in these measurements (2.71 eV, 457 nm), the excitation should involve just one photon. Besides that, a stronger luminescence signal is observed in the near-infrared region and it increases as the Au-NPs decrease. According to the literature, the above two emission bands in the visible and infrared can be attributed to interband and intraband radiative transitions involving electrons in the sp-conduction band and holes in the d-band of NPs^{21,23,29}. However, NPs embedded in a-Si:H has a different behaviour since the emitted photons can be absorbed by gap states of a-Si:H, followed by recombination or it can induce radiative transitions in the a-Si:H. That would explain the difference in the PL intensity of a-Si:H with Au-NPs 2 nm and Au-NPs 5 and 7 nm. In this analysis we exclude any effect of a-Si:H induced recrystallization during the film deposition, since micro Raman and spectroscopic ellipsometry measurements were performed (standard techniques to evaluate the crystallinity of Si:H film) and no difference was observed in samples with and without NPs. Although the a-Si:H deposited on 7 nm Au layers has high photoluminescence in the near infrared region the low transmission in the visible range unsuited its application to front layers of solar cells.

Overall, we showed a straightforward method to deposit Au-NPs with controllable particle size which consists in the deposition of very thin Au layer by thermal evaporation in heated substrates. The a-Si:H films deposited on Au-NPs layers has enhanced absorption in the infrared region (700–900 nm) opening doors to enhance amorphous silicon based solar cells efficiency through improvement of absorption close to the band gap of silicon and up-conversion of photons. The deposition of NPs can be made in any part of the solar cell, intra or inter layers, according to the size of NPs, by a compatible process.

Methods

Preparation of the Au-NPs and a-Si:H films. Au-NPs were deposited onto glass substrates by e-beam evaporation at substrate temperature of 250°C and deposition rate of 0.1–0.2 nm/s. The layer thickness was controlled, after opening the shutter of the system, by the deposition time and by a calibrated quartz crystal detector. This procedure enable the control of the layer thickness and three different layers were reproduced (2, 5 and 7 nm).

A 200 nm film of hydrogenated amorphous silicon (a-Si:H) was deposited by radio frequency plasma enhanced chemical vapour deposition (RF-PECVD) on the samples (2, 5 and 7 nm layers). During the a-Si:H deposition (20 min) the substrate was heated to 150°C. Details about the a-Si:H films can be found in previous works^{30,31}.

Structural and morphological characterization. To estimate the crystallite size and discard eventual cross-contaminations during the depositions, X-ray diffraction (XRD) measurements of the samples were performed in Panalytical X'Pert PRO with Cu K α line radiation ($\lambda = 1.540598 \text{ \AA}$) using the Bragg-Brentano configuration with a 2Theta range of 15 to 80° and a step size of 0.02°.

The SEM images of samples were performed in a Zeiss Auriga Crossbeam microscope with a Schottky Field Emitter column. The Everhart-Thornley type SE and InLens detectors were used with an aperture size of 30.00 μm , working distance between 4.8 and 5.6 mm and an acceleration voltage from 1 to 20 kV. The transmission electron microscopy (TEM) was performed in a Hitachi H-8100 microscope which runs at 200 kV in samples deposited directly in the Cu TEM grid with 400 nm mesh.

Optical characterization. The transmittance and reflectance spectra were obtained in double beam UV-VIS-NIR Shimadzu spectrophotometer with an integrating



sphere for reflectance and total transmittance measurements, in the range of 300–800 nm. The specular transmittance was measured in the range of and 300–2500 nm.

The PL measurements were performed both in the visible and in the infrared regions. In the first case, a Spex 1704 monochromator fitted with a cooled Hamamatsu R928 photomultiplier was used. The excitation source was the 457 nm line of a Melles–Griot laser with a power of ~30 mW. In the second region, a Bruker IFS 66v Fourier transform infrared (FTIR) spectrometer, equipped with a Ge diode detector, was used. The excitation source was a 514.5 nm line of an Ar⁺ ion laser, with a power of 151 mW. The samples were always inserted in a helium gas flow cryostat to allow the change of the temperature in the range 69–300 K. The excitation power was measured at the front of the cryostat window.

- Akimov, Y. A., Koh, W. S. & Ostrikov, K. Enhancement of optical absorption in thin-film solar cells through the excitation of higher-order nanoparticle plasmon modes. *Optics Express*, **17** (12), 10195 (2009).
- Pillai, S. & Green, M. A. Plasmonics for photovoltaic applications. *Solar Energy Materials & Solar Cells* **94**, 1481–1486 (2010).
- Hägglund, C. & Kasemo, B. Nanoparticle Plasmonics for 2D-Photovoltaics: Mechanisms, optimization, and Limits. *Optics Express* **17** (14), 11944 (2009).
- Losurdo, M., Giangregorio, M. M., Bianco, G. V., Sacchetti, A., Capezzuto, P. & Bruno, G. Enhanced absorption in Au nanoparticles/a-Si:H/c-Si heterojunction solar cells exploiting Au surface plasmon resonance. *Solar Energy Materials & Solar Cells* **93**, 1749–1754 (2009).
- Green, M. A., Emery, K., Hishikawa, Y. & Warta, W. *Prog. Photovolt: Res. Appl.* **19**, 84–92 (2011).
- Kelly, K. L., Coronado, E., Zhao, L. L. & Schatz, G. C. The Optical Properties of Metal Nanoparticles: The Influence of Size, Shape, and Dielectric Environment. *J. Phys. Chem. B* **107**, 668–677 (2003).
- Coronado, E. A., Ezequiel, R. E. & Stefani, F. D. Optical properties of metallic nanoparticles: manipulation light, heat and forces at the nanoscale. *Nanoscale* **3**, 4002–4059 (2011).
- Pillai, S., Catchpole, K. R., Trupke, T. & Green, M. A. Surface plasmon enhanced silicon solar cells. *J. Appl. Phys.* **101**, 093105 (2007).
- Akimov, Y. A. & Koh, W. S. Design of Plasmonic Nanoparticles for Efficient Subwavelength Light Trapping in Thin-Film Solar Cells. *Plasmonics* **6**, 155–161 (2011).
- El-Sayed, M. A. Some Interesting Properties of Metals Confined in Time and Nanometer Space of Different Shapes. *Acc. Chem. Res.* **34** (4), 257– (2001).
- Fahr, S., Rockstuhl, C. & Lederer, F. Improving the efficiency of thin film tandem solar cells by plasmonic intermediate reflectors. *Photonics and Nanostructures – Fundamentals and Applications* **8**, 291–296 (2010).
- Hutter, E. & Fendler, J. H. Exploitation of localized surface plasmon resonance. *Adv. Mat.* **16**, n19, 1685–1705 (2004).
- Nakayama, K., Tanabe, K. & Atwater, H. A. Plasmonic nanoparticle enhanced light absorption in GaAs solar cells. *App. Phys. Lett.* **93**, 121904 (2008).
- Li, Y., Peng, R., Xiu, X., Zhang, X. & Zhai, G. Growth of SnO₂ nanoparticles via thermal evaporation method. *Superlattices and Microstructures* **50**, 511–516 (2011).
- Chang, S.-S. & Park, D. K. Novel Sn powder preparation by spark processing and luminescence properties. *Mat. Sci. Eng. B* **95**, 55–60 (2002).
- Buonsanti, R., Llordes, A., Aloni, S., Helms, B. A. & Milliron, D. J. Tunable Infrared Absorption and Visible Transparency of Colloidal Aluminum-Doped Zinc Oxide Nanocrystals. *Nano Lett.* **11**, 4706–4710 (2011).
- Skrabalak, S. E., Au, L., Li, X. & Xia, Y. Facile Synthesis of Ag Nanocubes and Au Nanocages. *Nat. Protoc.* **2**, 2182–2190 (2007).
- Hutter, E. & Fendler, J. H. Exploitation of localized surface plasmon resonance. *Adv. Mat.* **16**, n19, 1685–1705 (2004).
- Iida, T. & Ishihara, H. Theoretical Study of the Optical Manipulation of Semiconductor nanoparticles under an Excitonic Resonance Condition. *Phys. Rev. Lett.* **90**, 057403 (2003).
- McMahon, M. D., Lopez, R., Meyer, H. M., Feldman, L. C. & Haglund, R. F. J. R. Rapid tarnishing of silver nanoparticles, in ambient laboratory air. *Appl. Phys. B* **80**, 915–921 (2005).
- Mooradian, A. Photoluminescence of Metals. *Phys. Rev. Lett.* **22**, 185–187 (1969).
- Link, S., Beeby, A., Fitzgerald, S., El-Sayed, M. A., Schaaff, T. G. & Whetten, R. L. Visible to Infrared Luminescence from a 28-Atom Gold Cluster. *J. Phys. Chem. B* **106**, 3410–3415 (2002).
- Zheng, J., Zhou, C., Yu, M. & Liu, J. Different Sized Luminescent Gold Nanoparticles. *Nanoscale* **4**, 4073–4083 (2012).
- Sun, H., Yu, M., Wang, G., Sun, X. & Lian, J. Temperature-Dependent Morphology Evolution and Surface Plasmon Absorption of Ultrathin Gold Island Films. *J. Phys. Chem. C* **116**, 9000–9008 (2012).
- Luth, H. In *Solid Surfaces and Interfaces Thin Films*, ed. by W. T. Rhodes, H. E. Stanley, R. Needs, Springer Heidelberg Dordrecht London New York, 2010, cap. 3.
- Halas, N. J., Lal, S., Chang, W. S., Link, S. & Nordlander, P. Plasmons in Strongly Coupled Metallic Nanostructures. *Chem. Rev.* **111**, 3913–3961 (2011).
- Sangita, J. A. & Sharma, R. P. A study of nanoellipsoids for thin-film plasmonic solar cell applications. *J. Phys. D: Appl. Phys.* **45**, 275101 (2012).
- Wilcoxon, J. P. & Martin, J. E. Photoluminescence from nanosize gold clusters. *J. Chem. Phys.* **108**, 9137 (1998).
- Link, S., Beeby, A., Gerald, S. F., El-Sayed, M. A., Schaaff, T. G. & Whetten, R. L. Visible to Infrared Luminescence from a 28-Atom Gold Cluster. *J. Phys. Chem. B* **106**, 3410 (2002).
- Martins, R., Raniero, L. & Pereira, L. *et al.* Nanostructured silicon and its application to solar cells, position sensors and thin film transistors. *Phil. Mag.* **89** (28–30), 2699–2721 (2009).
- Águas, H. & Martins, R. *et al.* Silicon thin film solar cells on commercial tiles. *Energy Environ. Sci.* **4**, 4620–4632 (2011).

Acknowledgments

The authors acknowledge to Strategic Project PEst-C/CTM/LA0025/2011 and QREN-5619 project and also to Joana Vaz Pinto and Luis Pereira for the XRD measurements and SEM images, respectively.

Author contributions

All the authors have contributed to the paper as follows: D.G. and A.C.P. have performed the deposition of Au layers and their optical characterization including statistics analysis of SEM images; T.M. and A.A. have produced the amorphous silicon layers and performed the electro-optical characterization; J.P.L., J.S. and B.P.F. have performed the PL measurements and interpreted the results; S.A.F. and H.Á. have made the interpretation of Au-NPs optical results; R. M. have contributed to writing the paper; I.F. is the mentor of the work performed.

Additional information

Competing financial interests: The authors declare no competing financial interests.

License: This work is licensed under a Creative Commons Attribution-NonCommercial-NoDerivs 3.0 Unported License. To view a copy of this license, visit <http://creativecommons.org/licenses/by-nc-nd/3.0/>

How to cite this article: Gaspar, D. *et al.* Influence of the layer thickness in plasmonic gold nanoparticles produced by thermal evaporation. *Sci. Rep.* **3**, 1469; DOI:10.1038/srep01469 (2013).